VIII ECCOMAS Thematic Conference on Smart Structures and Materials
SMART 2017
A. Güemes, A. Benjeddou , J. Rodellar and Jinsong Leng (Eds)

# HIGHLIGHTS AND CHALLENGES IN DAMAGE ASSESSMENT OF COMPOSITE STRUCTURES

**WIESŁAW OSTACHOWICZ*,†, PAWEŁ MALINOWSKI*, TOMASZ WANDOWSKI***

* Institute of Fluid Flow Machinery, Polish Academy of Sciences
Fiszera 14 St, 80-231Gdansk, Poland
e-mail: wieslaw@imp.gda.pl, https://www.imp.gda.pl/en/o4/z1/

† Warsaw University of Technology, Faculty of Automotive and Construction Machinery,
Narbutta 84 St, 02-524 Warsaw, Poland

**Key words:** Damage assessment, Composite structures, Bonded joints, Delaminations

**Abstract.** The paper presents multidisciplinary methods and techniques oriented towards damage identification and assessment in composite structures reinforced by carbon and glass fibres. A simulated damage in the form of teflon insert as well as real damage in the form of delamination were investigated. The paper reports applications of electromechanical impedance EMI and guided wave propagation methods. Presented methods are also suitable for performance of bonded joints assessment. Particularly the investigations concern contaminated bonds caused by both manufacturing (e.g. release agent) and in–service contaminations (e.g. de–icer). Techniques for detection of weak bonds are presented together with signal processing approaches.

## 1 INTRODUCTION

Nowadays aerospace structures are made more and more often out of various composite materials like glass/carbon fiber reinforced polymers (GFRPs, CFRPs) or glass laminate aluminum reinforced epoxy (GLARE). Due to this fact the up-to-date NDT techniques should handle with the wide range of these materials and potential defect types that could initiate and grow in such materials. Beside of typical damage like matrix cracking and delamination cause by impact [1],[2] attention should be focused on such a problems like for example the surface quality, the performance of structural bonds or moisture content. The process of adhesive bonding for aerospace structures nowadays is present at the manufacturing process as well as in service in the form of composite repair patches.
Nowadays composite structures need to be assessed using conventional NDT, extended NDT (ENDT) or SHM techniques in order to maximize the safety of exploitation of such structures what is very important in the case of aerospace structures. Still very popular methods are ultrasound testing (UT) method, Eddy current method or X-ray based methods. However, many other structural assessment methods have been developed. The examples are the

methods based on electromechanical impedance (EMI) or guided wave propagation (GW). Both techniques can be used in SHM when piezoelectric transducers are utilized for generation and sensing purposes. In the case of guided wave propagation this method could be used also utilized as NDT technique when non-contact measurements are conducted using laser scanning vibrometer whereas the guided wave excitation is realized using piezoelectric transducer.

Moreover external factors need to be considered is real SHM solutions. External factors have influence on measurement results for such methods like electromechanical impedance or guided wave propagation. Sensitivity of both method to temperature changes are reported in literature [3],[4]. Changing temperature causes changes in the measurements characteristics for the electromechanical impedance method. Temperature change is manifested as horizontal shift of frequency peaks [5],[6]. EMI method is also influenced by changing the load of investigated structure [6],[7]. In the case of guided wave based method, the velocity of guided wave propagation depends on material properties that on the other hand depends on temperature. As consequence velocity of guided wave propagation changes according to the temperature change. These features need to be taken into account in the SHM. Signal processing algorithm for compensation of temperature influence need to be utilized.

This paper is divided into two major sections. Firstly, the electromechanical impedance method and results are presented. Secondly, the guided wave propagation method based on laser vibrometry together with results are presented.

## 2 EMI METHOD

EMI method is based on measurements of electrical parameters of a piezoelectric transducer coupled with the investigated structure. Due to electromechanical coupling of piezoelectric transducer and the host structure, mechanical resonances of structure can be observed in electrical characteristics of piezoelectric transducer. Probably the first published record about the method was made by Liang et al. who proposed an one-dimensional equation [8].

In the EMI method electrical parameters like impedance, admittance, their real parts (respectively resistance and conductance) and their imaginary parts (reactance and susceptance) can be registered and analyzed. According to literature, imaginary part of electrical parameters is used for monitoring of bonding layer between transducer and structure or diagnosis of the transducer itself [9], while the real part of electrical parameters is utilized for monitoring of the structure. Reactance was utilized as a parameter that allows to detect transducer debonding, while the resistance was used for assessment of the structure [10]. However, also both the resistance and susceptance were used to detect sensor faults in other research [11].

### 2.1 Assessment of adhesive bonding by EMI

Samples that comprise of two adhesively bonded subsamples were investigated. The material used for subsamples manufacturing was Hexcel M21E with $[0, 0, 45, -45]_s$ layup. Each subsample had a planar size of 100 mm x 100 mm. These subsamples were bonded together with FM 300-2 adhesive film. Two cases of pre-bond modifications were investigated. The modified samples were compared against reference samples. The investigations included: 3 reference samples, 9 samples with pre-bond thermal treatment, 9 samples with pre-bond

contamination with de-icing fluid. The thermal treatment was performed by exposure of the samples to elevated temperatures before bonding. Three samples were prepared for each temperature: 220, 260, 280˚C. TD1, TD2 and TD3 sample symbols were assigned, respectively. The pre-bond contamination was prepared by dip coating of the plates in a water solution of the de-icer with three concentrations. After drying the potassium formiate, which is present in the de-icing fluid, forms a thin layer on the CFRP. The potassium (K) content measured with XPS was taken as a measure of contamination. The contamination resulted in three samples contaminated at 6.4 at.% of K (DI1 samples) and six samples contaminated at 10.9-12.0 at.% of K (DI2 samples).
The conductance spectra were measured for the samples in 3-5 MHz ran and the RMS index was calculated. The results are presented as a mean value for each level of modification. In order to make the comparison the mean RMS values were presented as a percent change in relation to the mean RMS value calculated for the reference samples. Figure 1 depicts the result for all the cases. An increasing value of RMS is observed. The samples treated at 220˚C differ for the reference by less than 20%, while samples treated at 280˚C have the largest value, exceeding 50 %. In the results for contamination with the de-icing fluid (DI) one can notice similar behaviour. The lover level of delamination (DI1 - 6.4 at.% of K) differ by lee than 20% from the reference case. The higher amount of contamination (DI2) results in an RMS value increase by more than 20%.

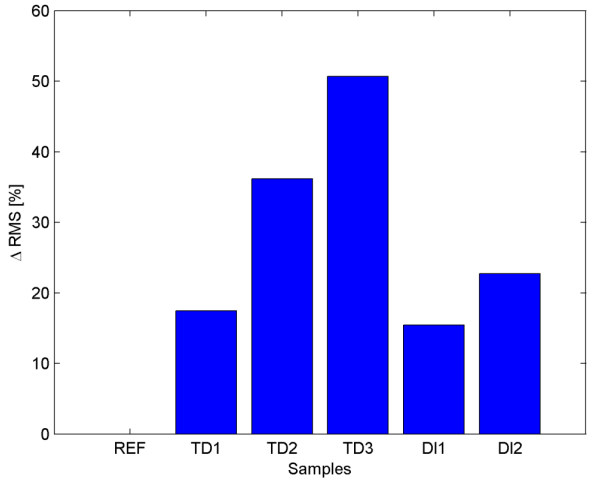


**Figure 1.** Relative RMS results for the samples with pre-bond thermal treatment (TD) and the samples with pre-bond de-icer contamination (DI)

## 2.2 Delamination detection by EMI

The EMI was also investigated for damage detection purposes. The investigated object was a 500 mm x 500 mm x 3 mm plate made of glass fibre reinforced polymer (GFRP sample) . The sample was made of 8 plies of biaxial fabric. In order to simulate damage a square (10 mm x 10 mm) teflon tape was inserted between the second and the third layer. The teflon was located in the right lower corner 120 mm away from the closest two edges. A network of four sensors were bonded to the sample surface. One sensor (P1) was bonded at the location of the

teflon insert The three remaining sensors (P1, P2, P3) were located symmetrically at the remaining three corners of the plate. We investigated the change of RMS value and the location of conductance maximum. The change was caused by bonding of the sensors and the state of the sample in the vicinity of the sensors. One can notice that after bonding the RMS value (energy) dropped for all cases (Figure 2). The drop is virtually uniform for the sensors P2-P4 bonded to the healthy part of the sample. However, there is a significant difference for P1 sensor that was bonded at the location of simulated delamination. In terms of frequency change one can notice that the frequency increases for P2 and P4 and decreases for P1 and P3 (Figure 3). However in terms of absolute values the change for P1 is the lowest, slightly lower than for the P4 sensor. The sensors located at the location of artificially made damage was clearly distinguish form the remaining cases. Teflon detection was successful.

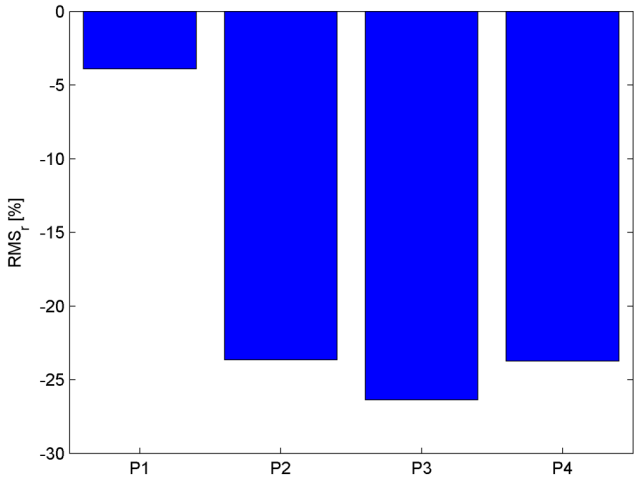


**Figure 2.** Relative conductance RMS change after bonding sensors (P1-P4) to the investigated GFRP sample

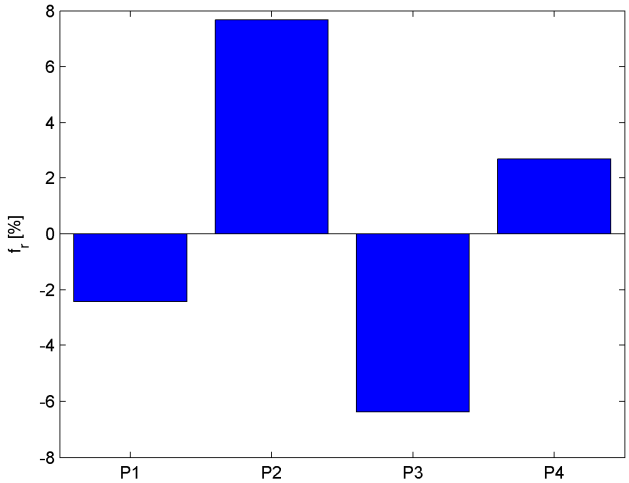


**Figure 3.** Relative change of conductance maximum peak frequency after bonding sensors (P1-P4) to the investigated GFRP sample

## 3 GUIDED WAVE PROPAGATION METHOD

This section is related to guided wave propagation method which can be utilized in the purpose of damage detection and localization. This method is based on the fact that any kind of discontinuities in structural element are the source of change in guided wave propagation. In the approach presented in this paper full wavefield method was utilized. The guided waves were excited using piezoelectric transducer (Noliac NCE51 piezoelectric disc with diameter 10 mm and thickness 0.5 mm) while the guided wave sensing process was conducted using Polytec Scanning Laser Doppler Vibrometer SLDV.

### 3.1 Simulated delaminations in GFRP samples

In the first step measurements were conducted for Glass Plastic Reinforced Polymer (GFRP) panel with dimensions 500 mm x 500 mm and thickness ~1.5 mm. Panel consists of twelve layers of VV192T/202 IMP503 prepregs with orientations: $[0/90/0/90/0/90]_S$. In this panel four circular teflon inserts, each with diameter 20 mm, were embedded between layers of lamina in order to simulate delaminations (Figure 4). Teflon inserts were located at different depth what can be noticed in the Figure 5.

**Figure 4.** View of GFRP sample no. 1

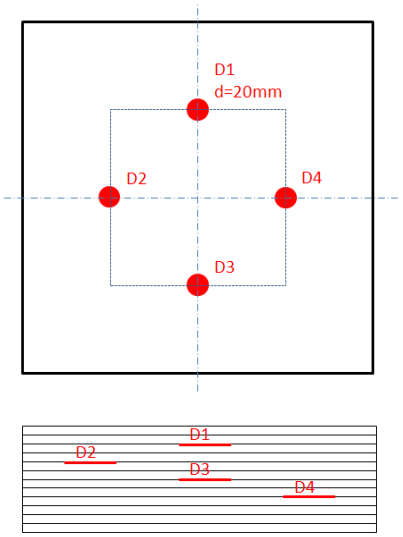


**Figure 5.** Teflon insert locations in the GFRP sample no. 1

In the Figure 6 results of full wavefield measurements in the form of frames chosen from animation of guided wave propagation were presented. Measurements were taken for excitation frequency 200 kHz. Analyzing results in Figure 6a) propagation of symmetric and antisymmetric fundamental modes S0 and A0 could be noticed. In the Figure 6b) interactions of S0 mode with teflon inserts could be noticed – mode S0 is converted to A0' mode. The amplitude of A0' mode (as result of mode conversion) depends on the depth at which teflon insert was inserted. Amplitude of A0' mode is largest in the case of teflon insert denoted as D1 that is located below second layer counting from top of the panel where the measurements were performed.

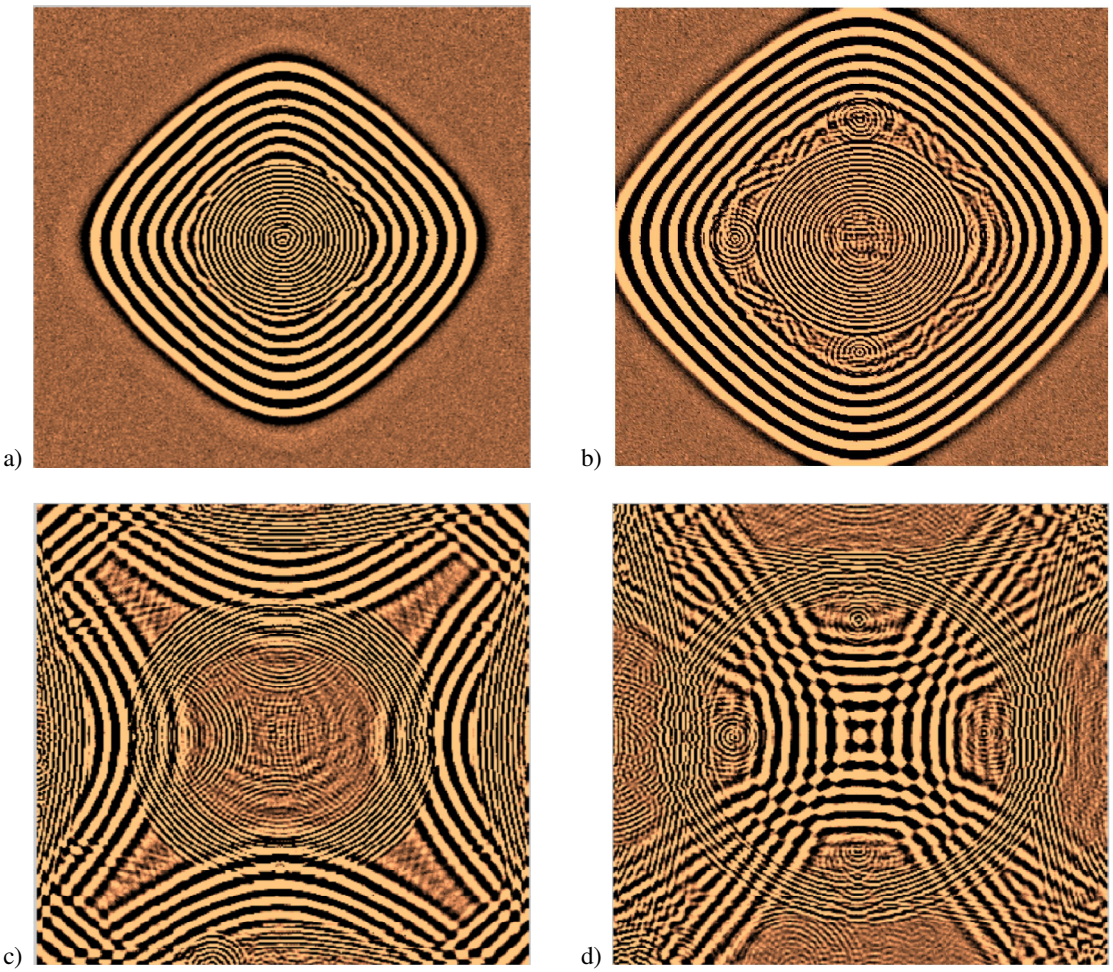


**Figure 6.** Selected frames from animation of guided wave propagation in GFRP sample no.1: a-d) subsequent frames

Amplitude of A0'mode is smallest amplitude for the teflon insert denoted as D4 which is located eight layers from the top (deepest). What is interesting, mode conversion phenomenon is clearly visible for the case of teflon insert denoted as D3, which is placed symmetrically in respect to the panel thickness. According to the literature mode conversion phenomenon occurs only for the discontinuities placed non-symmetrically in respect to the thickness of composite laminate. This fact was proved by the numerical simulations which results were published in [12]. Numerical result for carbon fibre reinforced polymer CFRP showed that there is no mode conversion in the case of symmetrically placed delamination (simulated by node separation in the spectral elements). In the case of experimental results for CFRP panel presented in the paper [12] mode conversion occurred for symmetrically as well non-symmetrically placed delamination (simulated by teflon insert). These experimental result for CFRP panel agree with results for GFRP panel presented here. According to the paper [13] the existence of discontinuity destroys the symmetry of the wave, resulting in mode conversion. It means that location of delamination never is perfectly symmetrical in the

relation to the panel thickness. This is obvious for real structures where it is hard to achieve ideal symmetry.

In the Figure 6c) S0 to A0 mode conversion phenomenon could be noticed as a consequence of S0 interaction with panel boundaries. In the Figure 6d) reflections of A0 mode from teflon inserts could be noticed. After carefully analysis of results presented in Figure 6c) and Figure 6d) additional local S0/A0' mode conversion could be noticed in the point located at the bottom panel edge. There was very small notch at panel surface just on the edge which caused mode conversion phenomenon.

In the next step signal processing algorithm was utilized in order to visualize the simulated delamination locations. The simply and widely used full wavefield signal processing is calculation of Weighted Root Mean Square (WRMS) for the time domain signals at discrete time interval. As consequence energy distribution related to propagation of wave and its interaction with discontinuities in the structure is obtained. In the WRMS algorithm weight factor is utilized which decreases the importance of the time samples at the beginning when excitation is applied (large wave amplitudes) and increases the importance of the samples closer to the end of signal where waves amplitudes are small due to damping. The Weighted Root Mean Square (WRMS) can be calculated using formula:

$$WRMS = \sqrt{\frac{1}{N}\sum_{k=1}^{N} w_k s^2} \tag{1}$$

where the weighting factor $w_k$ is defined as follows:

$$w_k = k^m, \quad m \geq 0 \tag{2}$$

In the Figure 7 WRMS energy maps for guided wave propagation in the GFRP panel with four circular teflon inserts (Figure 4 and Figure 5) were presented. Both WRMS energy maps were constructed for the excitation frequency 200 kHz.

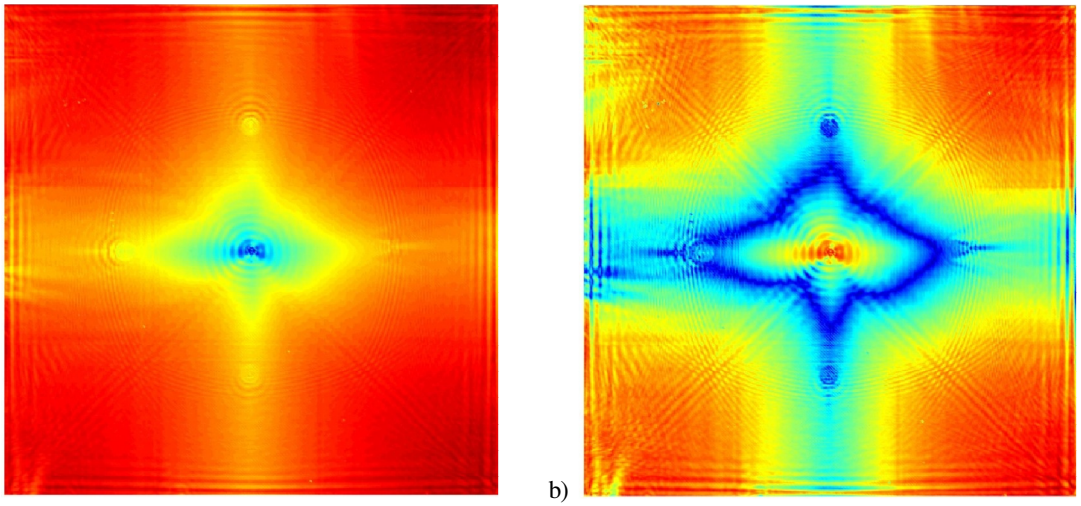

a) b)

**Figure 7.** WRMS guided wave energy maps for: a) *m*=0.1, b) *m*=0.65; GFRP sample no. 1

Energy map in the Figure 7a) was constructed for parameter *m* equal to 0.1. Locations of four circular teflon inserts can be easily noticed analyzing of guided wave energy concentrations near the defects. Moreover, strong energy concentration along angles $0^o$ and $90^o$ could be noticed. This is caused by orientation of glass fabric reinforcement in the panel.
Energy map presented in the Figure 7b) was constructed for parameter *m* equalto 0.65. In this case change of energy distribution due to teflon inserts as well as orientation of glass fabric reinforcement is much more visible.
Analogus measurements and signal processing were performed for second GFRP sample. This sample was manufactures using the same material like sample no. 1 and using the same number of layers and its orientations. In this sample planar locations of teflon inserts were changed (Figure 9). Now the inserts are not located at directions $0^o$ and $90^o$ along which strong energy concetration occurs. In the Figure 9 selected frame presenting propagation of S0 and A0 modes in this sample was showed. Measurements were taken for excitation frequency 200 kHz. In this case S0/A0' mode conversion phenomenon in the regions were teflon inserts were located can be also noticed. However, amplitudes of A0' mode generated in the consequence of S0 mode conversion are lower than in the case of previous sample. In this case amplitudes of A0' mode also depends on the deept were the insert was located.

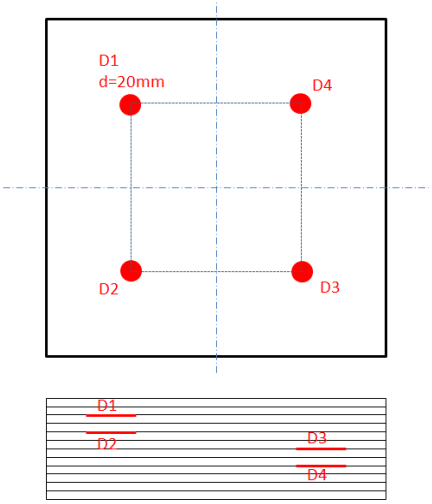


**Figure 8.** Teflon insert locations in the GFRP sample no. 2

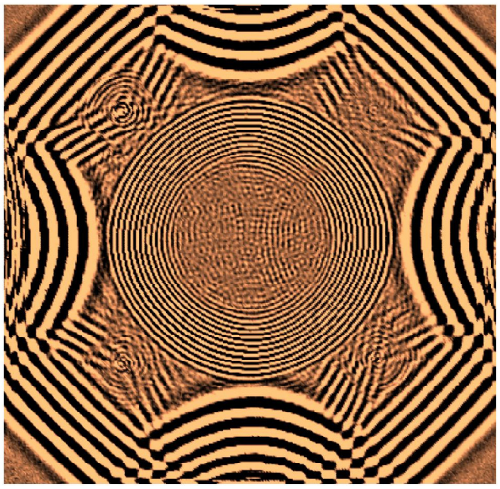

**Figure 9.** Selected frame from animation of guided wave propagation in GFRP sample no. 2

In the next step WRMS energy maps for coeeficient *m* equal to 0.1 and 0.65 were constructed – see Figure 10a) and Figure 10b) respectively. In the case of *m*=0.1 changes of energy distribution caused by teflon inserts are amost invisible (Figure 10a)). Locations of teflon inserts denoted D1-D3 could be noticed in the case of WRMS energy map constructed for *m*=0.65. Location of insert D4 is almost invisible – it is the deepest insert in the panel.

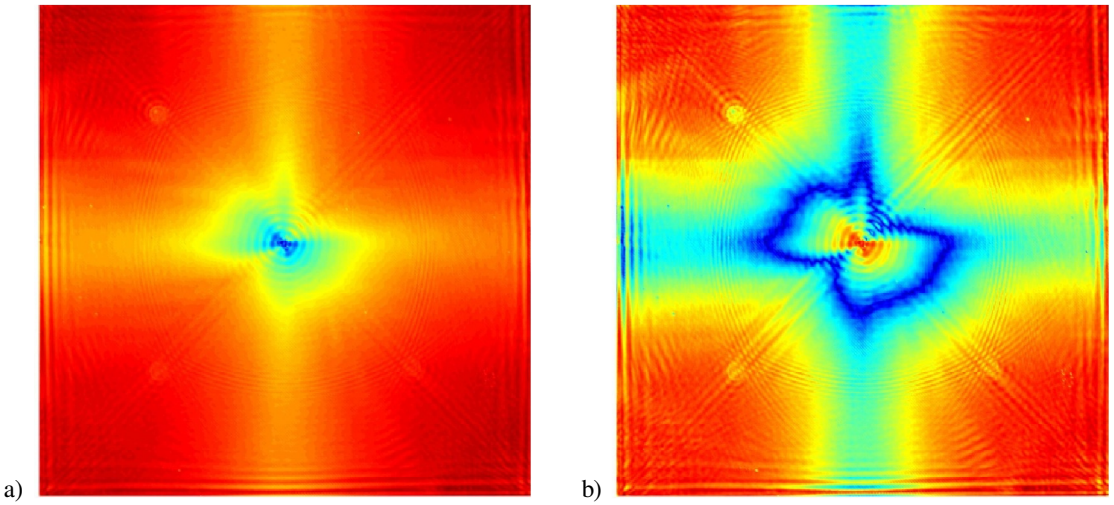

**Figure 10.** WRMS guided wave energy maps for: a) $m$=0.1, b) $m$=0.65; GFRP sample no. 2

In the further research third GFRP sample was utilized (Figure 11). This sample was manufactures using the same material like sample no. 1 and no. 2 using the same number of layers and the same orientations. In this case influence of different shapes of teflon on the guided wave propagation was investigated. All teflon inserts were located at the same depth (Figure 12).

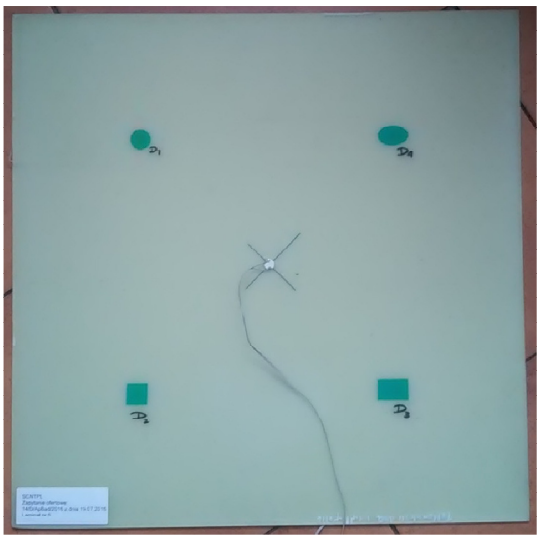

**Figure 11.** View of GFRP sample no.3

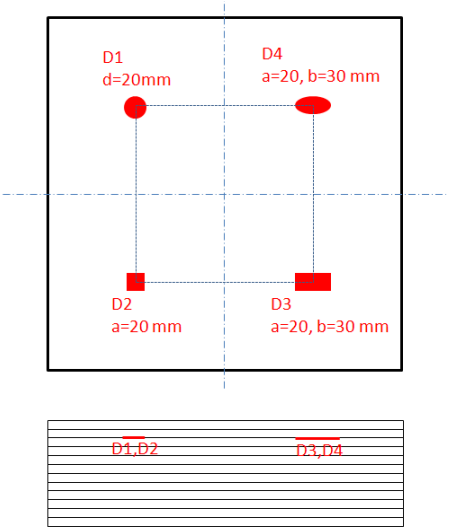


**Figure 12.** Teflon insert locations in the GFRP sample no. 3

In the Figure 13 selected frame presenting propagation of S0 and A0 modes for excitation frequency 200 kHz in the GFRP sample no. 3 was showed. This frame was selected because it clearly shows interactions of S0 mode with teflon inserts with different shapes. Due to interaction of S0 mode with teflon inserts, phenomenon of S0/A0' mode conversions is observed. In the Figure 14 magnifications of wavefield around teflon inserts were presented.

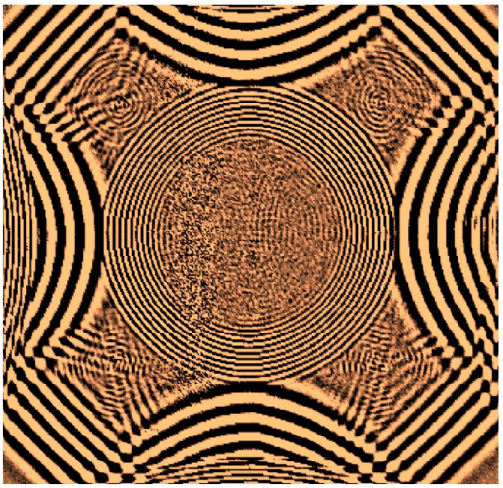

**Figure 13.** Selected frame from animation of guided wave propagation in GFRP sample no. 3

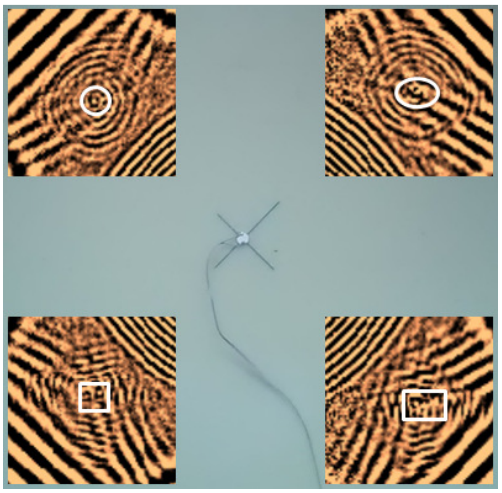

**Figure 14.** Wavefield around the teflon inserts capturing – S0/A0' mode conversion - GFRP sample no. 3

Analyzing wavefield around each teflon insert it can be observed that wavefront of new A0' mode depends on the shape of teflon insert. In the case of circular and elliptical insert wavefront has circular and elliptical shape. In the case of square and rectangular we could notice that wavefront is formed on the edges of teflon insert. Moreover, entrapment of A0' mode in the region of teflon insert is also observed. Similar effects were observed in [12], [14].

a) b)

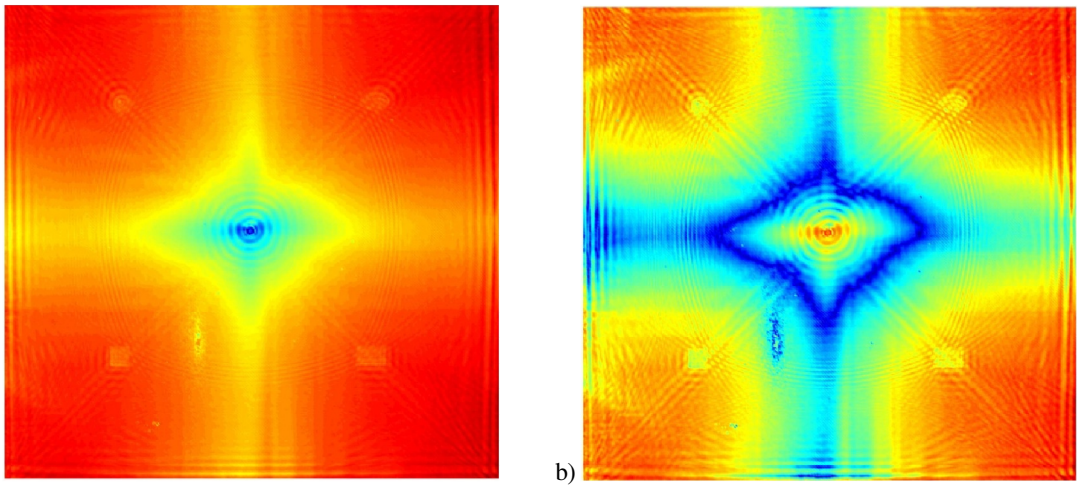

**Figure 15.** WRMS guided wave energy maps for: a) $m$=0.1, b) $m$=0.65; GFRP sample no. 3

In the next step WRMS energy maps for GFRP sample no. 3 and coefficient $m$ equal 0.1 and 0.65 were constructed – see Figure 15a) and Figure 15b) respectively. Energy map presented in Figure 15a) indicates clearly the shapes of all embedded in panel teflon inserts.

Utilization of higher values of *m* coefficient (0.65) allows to improve slightly the contrast between referential regions of sample and regions with teflon inserts. It should be underlined that in this case teflon inserts were located out of the directions of glass fabric reinforcements oriented at angles $0^o$ and $90^o$.

### 3.2 Delamination in CFRP L-shape sample

In previous section authors investigated GFRP samples with teflon inserts simulating delaminations. The aim of research was to investigate the interactions of guided wave modes with discontinuities with different shapes and locations (planar as well as in the thickness).
In this sections results of investigation of guided wave interaction with true delamination in CFRP panel were presented. Panel were made out of 16 layers of CFRP pre–pregs GG204P IMP503 42 with following orientations $[0/90/0/90/0/90/0/90]_S$. Total thickness of panel was ~3.5 mm. From rectangular panel, smaller rectangular section was cut-off using water jet, creating L-shape panel. During water jet cutting process large delamination was created in the corner. In this delamination two layers of prepreg, counting from the top of panel were separated from the rest part of the panel. Total thickness of two layer was ~0.4 mm.
In the Figure 16 selected frames taken from animation of guided wave propagation in L-shape CFRP panel with delamination were presented. Guided waves were excited using piezoelectric transducer located at the middle of the bottom edge of panel. In this case excitation frequency was equal 200 kHz. Measurement were taken at the top surface using laser vibrometer.

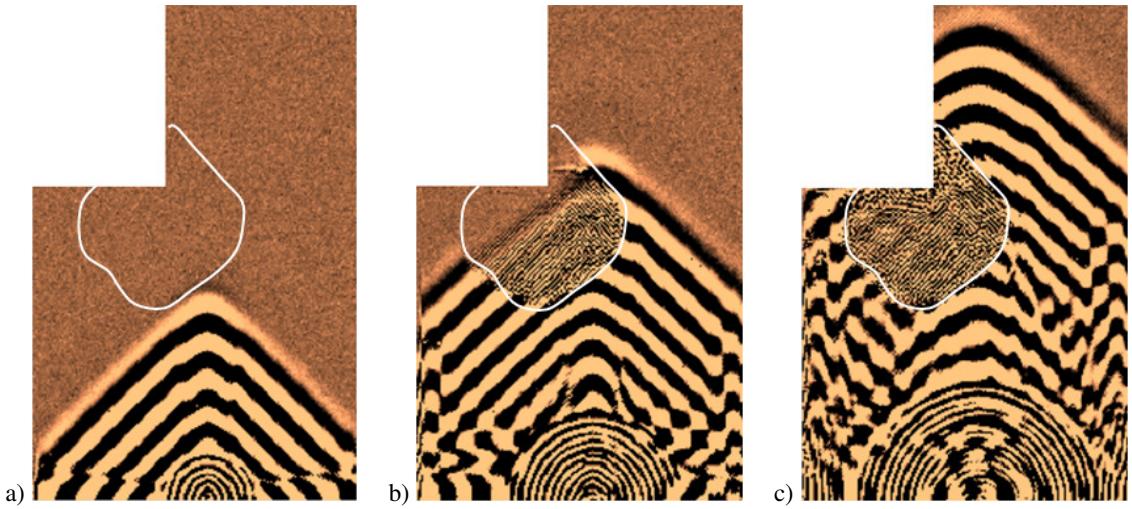


**Figure 16.** Selected frames from animation of guided wave propagation in L-shape CFRP sample with delamination

Analyzing frame presented in Figure 16a) propagation of S0 and A0 modes can be observed. Both modes could be simple distinguished. Mode S0 propagate with higher velocity than A0 mode and has larger wavelength. In the frame presented Figure 16b) interaction of S0 mode with delamination could be observed. Approximated shape of delamination located in the corner is marked by white curve. In the delaminated region propagation of two wave modes

can be observed: mode with length comparable to S0 and mode with much smaller wavelength than S0 and also slightly smaller than A0 – called here A0'. The second mode results from mode conversion phenomenon. In the Figure 16c) propagation of mode with smaller wavelength than A0 could be observed. Moreover, phenomenon of entrapment of A0' mode in the delaminated region of panel is clearly visible.

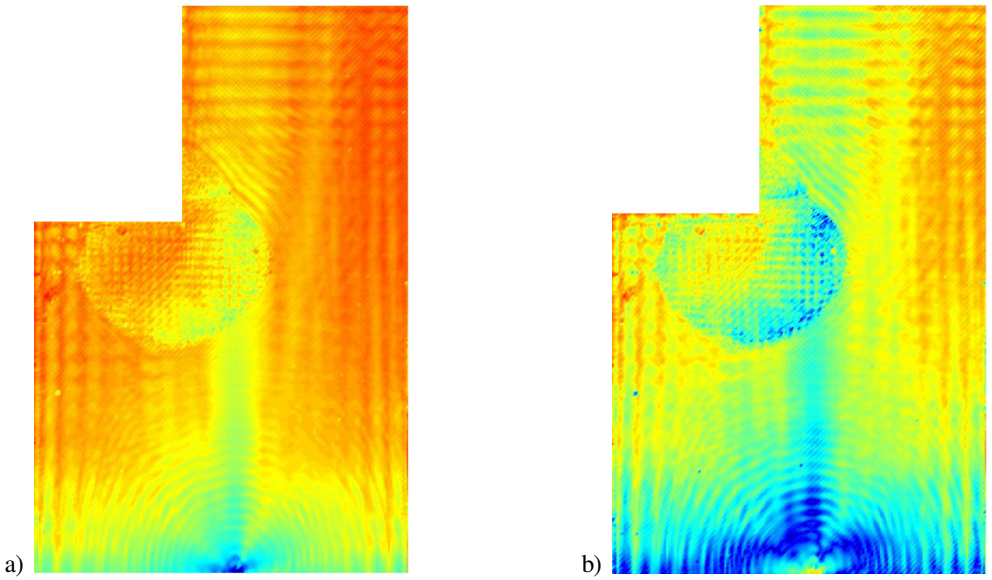


**Figure 17.** WRMS guided wave energy maps for: a) *m*=0.1, b) *m*=0.65; L-shape CFRP sample with delamination (measurements at top surface)

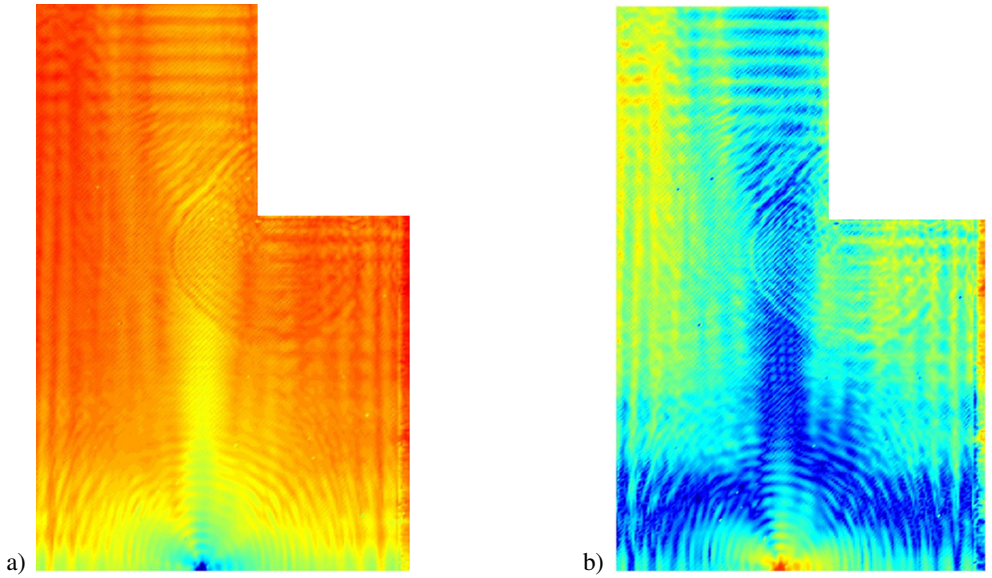


**Figure 18.** WRMS guided wave energy maps for: a) *m*=0.1, b) *m*=0.65; L-shape CFRP sample with delamination (measurements at bottom surface)

Next step was related to construction of WRMS energy map for propagating elastic waves.
In the Figure 17a) and Figure 17b) WRMS energy maps constructed respectively for the coefficient values 0.1 and 0.65 were presented. In both cases analyzing WRMS energy maps, delaminated region could be easily distinguished.
In next step measurements were taken at the bottom surface of panel. At this side of the panel thickness of material in the delaminated zone is equal ~3.1 (14 layers of prepregs). In the Figure 18a) and Figure 18b) WRMS energy maps for guided wave propagation were constructed for the *m* coefficient equal respectively to 0.1 and 0.65. Delaminated region could be distinguished in both presented cases in Figure 18. However, the contrast of energy distribution in delaminated and referential region is not so high like in previous case (measurements on the top surface).
Results presented in this section shows that proposed damage localization approach based on WRMS energy maps works properly not only in the case of artificially simulated defect using teflon insert but also in the case of real delamination.

## 4 CONCLUSIONS

It was shown that the EMI method indicates some sensitivity to the modification of adhesive bonds of CFRP samples. There is an increase in RMS index as the modification severity is higher so the bond quality level determination could be possible. This was observed both for thermally treated samples and contaminated with de-icing fluid.
It was shown that the EMI method is sensitive to a delamination simulated by a teflon insert. The change of RMS value clearly indicates which of the sensors is located on 'damaged' material. The change of the RMS is the lowest for this case. This suggest that delamination causes that only two layers of GFRP interacts with the sensor allowing it to vibrate more freely than in the remaining cases where the sensors is bonded to a 8-layer thick part of the plate.
Moreover, damage localisation algorithm based on WRMS energy maps was verified for the case of simulated delaminations (using teflon inserts) as well as in the case of true delamination. Utilization of teflon insert allowed to investigate influence of simulated damage location (planar and in the thickness) and its shape on guided wave mode interactions with it. Attention was focused on the phenomenon of S0/A0' mode conversion due to interaction of elastic wave with teflon inserts. Results showed that amplitude of A0' mode created as result of S0 mode conversion depends on the depth where the teflon insert is located. Mode conversion phenomenon occurs even for the case of teflon layer placed symmetrically in the respect to panel thickness. Radiated wave field for A0' mode is strictly related to the shape of teflon inserts. Moreover, entrapment effect for A0' mode was noticed. This effect was observed in the regions where teflon inserts were located. Utilisation of interactions of A0 and S0 mode with teflon inserts allow to localise the planar location of insert and to identify its shape. In this case WRMS energy maps were utilized.
In the next step sample with true delamination was investigated. In this case mode conversion phenomenon was also observed. Application of WRMS energy map based damage localisation algorithm allow to localise the location of delamination and identify its approximated shape.

## ACKNOWLEDGEMENTS

Authors would like to gratefully acknowledge financial support given by National Science Centre, Poland by the decision no. DEC-2013/11/D/ST8/03355.
Authors would like to gratefully acknowledge financial support under grant agreement no. UMO-2014/13/D/ST8/03167 in the frame of SONATA project entitled: "Investigation of elastic wave mode conversion phenomenon in thin-walled structures with discontinuities".
The research was funded by the Polish National Science Centre under grant agreement no DEC-2013/10/A/ST8/00071 in the frame of MAESTRO project entitled: Excitation and control of mechanical waves in nonlinear media.
Part of this research has received funding from the European Union's Horizon 2020 research and innovation programme under grant agreement No 636494 (project entitled: "Quality assurance concepts for adhesive bonding of aircraft composite structures by advanced NDT - ComBoNDT").

## REFERENCES

[1] Tian, Z., Yu, L. and Leckey, C. Delamination detection and quantification on laminated composite structures with Lamb waves and wavenumber analysis. *Journal of Intelligent Material Systems and Structures* (2015) 26(13): 1723-1738.

[2] Ren, Y., Qiu, L. Yuan, S. and Su, Z.: A diagnostic imaging approach for online characterization of multi-impact in aircraft composite structures based on a scanning spatial-wavenumber filter of guided wave. *Mechanical Systems and Signal Processing* (2017) 90: 44-63.

[3] Grisso, B.L. and Inman, D.J. Temperature corrected sensor diagnostics for impedance-based SHM. *Journal of Sound and Vibration* (2010) 329, 2323–2336.

[4] Baptista, F.G., Budoya, D.E., Almeida, V.A. and Ulson, J.A. An experimental study on the effect of temperature on piezoelectric sensors for impedance-based Structural Health Monitoring. *Sensors* (2014) 14, 1208-1227.

[5] Lim, H.J., Kim, M.K., Sohn, H. and Park, C.Y. Impedance based damage detection under varying temperature and loading conditions. *NDT&E International* (2011) 44:740–750.

[6] Annamdas, V.G.M., Yang, Y. and Soh, C.K. Influence of loading on the electromechanical admittance of piezoceramic transducers. *Smart Materials and Structures* (2007) 16.

[7] Benmeddour, F., Grondel, S., Assaad, J. and Moulin, E. Experimental study of the $A_0$ and $S_0$ Lamb waves interaction with symmetrical notches. *Ultrasonics* (2009) 49(2): 202-205.

[8] Liang, C, Sun, F.P., Rogers, C.A. Coupled electro-mechanical analysis of adaptive material system—determination of the actuator power consumption and system energy transfer. *J. Intell. Mater. Syst. Struct.* (1994) 5: 12-20.

[9] Park, G., Farrar, C.R., Lanza di Scalea, F. and Coccia, S. Performance Assessment and Validation of Piezoelectric Active-Sensors in Structural Health Monitoring. *Smart Mater. Struct.* (2006) 15(6): 1673–1683.

[10] Giurgiutiu, V. *Structural Health Monitoring with piezoelectric wafer active sensors*. Elsevier, Academic Press (2008).

[11] Buethe, I., Moix–Bonet, M., Wierach, P. and Fritzen, C.-P. Check of Piezoelectric Transducers Using the Electro–Mechanical Impedance. *Proc. 7th European Workshop on Structural Health Monitoring* (2014), Nantes, France.

[12] Wandowski, T., Kudela, P., Malinowski, P. and Ostachowicz, W. Defect induced guided waves mode conversion. *Proc. SPIE 9805, Health Monitoring of Structural and Biological Systems 2016*, 98050O (2016), doi:10.1117/12.2218233

[13] Jin, J., Quek, S.T. and Wang, Q. Wave boundary element to study Lamb wave propagation in plates. Journal of Sound and Vibration (2005) 288: 195–213.
[14] Tian, Z., Leckey, C., Yu, L., Seebo, J.P. Impact induced delamination detection and quantification with guided wavefield analysis. *Proc. SPIE 9435*, (2015); doi:10.1117/12.2083358